Journal of Materials Chemistry A

PAPER

View Article Online
View Journal | View Issue

Cite this: J. Mater. Chem. A, 2014, 2, 5399

Understanding the electrochemical mechanism of the core–shell ceria–LiZnO nanocomposite in a low temperature solid oxide fuel cell

Liangdong Fan,[ab] Ying Ma,[c] Xiaodi Wang,[d] Manish Singh[b] and Bin Zhu*[ab]

Received 11th October 2013
Accepted 19th January 2014

DOI: 10.1039/c3ta14098a

www.rsc.org/MaterialsA

Ceria based solid solutions have been considered some of the best candidates to develop intermediate/low temperature solid oxide fuel cells (IT/LT-SOFCs, 600–800 °C). However, the barrier to commercialization has not been overcome even after numerous research activities due to its inherent electronic conduction in a reducing atmosphere and inadequate ionic conductivity at low temperatures. The present work reports a new type of all-oxide nanocomposite electrolyte material based on a semiconductor, Li-doped ZnO (Li_xZnO), and an ionic conductor, samarium doped ceria (SDC). This electrolyte exhibits superionic conductivity (>0.1 S cm^{-1} over 300 °C), net-electron free and excellent electrolytic performances (400–630 mW cm^{-2}) between 480 and 550 °C. Particularly, defects related to interfacial conduction and the intrinsic and extrinsic properties of ions are analysed. An internal or interfacial redox process on two-phase particles is suggested as a powerful methodology to overcome the internal short-circuit problem of ceria-based single phase materials and to develop new advanced materials for energy related applications. The combination of the above promising features makes the SDC–LiZnO nanocomposite a promising electrolyte for LTSOFCs.

Introduction

As one of the most efficient and environmentally benign energy conversion devices, solid oxide fuel cells (SOFCs) have attracted much attention in recent years due to the high energy conversion efficiency, wide application range (both stationary and portable electronic energy supply), and fuel flexibility. Unfortunately, conventional SOFCs based on yttria-stabilized zirconia (YSZ) as the solid electrolyte require a high operating temperature (800–1000 °C), which results in high cost and insufficient lifespan, which are the main reasons for their limited commercialization to date. Therefore, there is an urgent need for low temperature operation, say below 600 °C, because inexpensive materials and cost-effective methodologies can be employed in this temperature range to develop marketable products.[1] Different strategies and cell fabrication technologies, such as reduction of the electrolyte thickness[2–4] (down to the nanometer level), the cell material[5–8] and microstructure optimization (porosity and tortuosity),[9,10] have been employed to make the zirconia based electrolyte more robust at reduced temperatures. But the complex processing technology and reduced mechanical strength cause difficulties in their wide implementation and cost reduction as well.

The alternative method is to achieve high ionic conductivity of the electrolyte at reduced temperatures.[11,12] Doped ceria has been considered as a suitable electrolyte candidate in the intermediate temperature range.[10,11,13,14] However, it shows significant electronic conductivity at lower oxygen partial pressures which results in a significant power loss. Besides, inadequate ionic conductivity at low temperatures, less than 600 °C, has further prevented its commercialization.[15] Lack of reliable electrolyte materials for low-temperature operation is thus a big challenge in the field of SOFCs.

In recent years, there has been an ever-growing interest in the development of composite electrolyte materials by using a functional composite or nanocomposite approach for advanced fuel cell technology (NANOCOFC, http://www.nanocofc.com).[16–18] There have been worldwide research activities on ceria-based composites as new superionic conducting electrolytes for LTSOFCs, operating in the temperature range of 300–600 °C.[19–28] The core–shell SDC–Na_2CO_3 nanocomposite, as a typical example, has been successfully developed and given excellent electrochemical performance and unique hybrid proton/oxygen ion conduction below 600 °C.[20] An outstanding power density of 1200 mW cm^{-2} has been achieved with a 250 μm thickness of an SDC–$(Li/Na)_2CO_3$ electrolyte at 600 °C.[22] The new architectures in nanocomposites yield

[a]Hubei Collaborative Innovation Center for Advanced Organic Chemical Materials, Faculty of Physics and Electronic Technology, Hubei University, Wuhan 430062, P.R. China. E-mail: zhubin@hubu.edu.cn; liangd_fan@hotmail.com

[b]Department of Energy Technology, Royal Institute of Technology (KTH), S-100 44 Stockholm, Sweden. E-mail: binzhu@kth.se

[c]Department of Applied Physics, Aalto University School of Science, FI-00076 AALTO, Finland

[d]Functional Materials Division, Royal Institute of Technology (KTH), S-164 40 Stockholm, Sweden

interesting properties with better conductivities, resulting from both unique nanomaterial blocks and two-phase interfaces. It has been demonstrated that the interfaces between ceria and the second constituent phase act as ionic conduction highways, leading to a superionic conductivity.[28,29] Manipulation of interfaces in these ceria-based nanocomposite materials, without the structural limitation, has tremendously reduced the working temperature of SOFCs from 1000 °C to 300–600 °C and led to the exploration of new science and technological opportunities to overcome the current SOFC challenges.[17,30] Employment of the second phase, normally salts, such as carbonates, also effectively suppresses the electronic conduction that takes place in ceria based single phase materials, especially at the anode surface.

Research on ceria-based composites has so far focused on ceria and salt two-phase composites. However, there is often an argument on the corrosion and stability of salts, *e.g.* carbonates, which were assumed to lead to the deterioration of fuel cell performance. An all-oxide composite electrolyte is expected to be a solution because of a more stabilized structure. In our recent studies, there have been some attempts to use all-oxide composites, *e.g.* SDC–BCY ($BaCe_{0.8}Y_{0.2}O_{2.9}$),[31] SDC–LiZnO (ref. 32) and SDC–Y_2O_3,[33] in which, SDC–LiZnO showed the most noticeable properties: a typical core–shell structure, excellent electrical conductivity and an extremely low ionic transport activation energy, excellent fuel cell performance (>600 mW cm^{-2} at 520 °C) and a superionic phase transition point around 350 °C.[32] In this work, we aim to further optimize the composition to improve the ionic conductivity and fuel cell performance. Particular attention is given to the interfacial nature from the defect chemistry aspect. A novel scientific approach is also proposed to explain the net-electron free phenomenon considering the co-electron and hole conduction of this novel all-oxide SDC–Li_xZnO nanocomposite. The interfacial super-conduction and internal redox process are the key points in the rational design and development of functional nanocomposite materials for LTSOFCs and other advanced energy conversion technologies.

Experimental

Both cerium nitrate hexahydrate (Sigma-Aldrich) and samarium(III) nitrate hexahydrate (Aldrich) solutions (0.5 M) were prepared separately. The two solutions were then mixed in a desired molar ratio ($Sm_{0.2}Ce_{0.8}O_{1.9}$) by mechanical stirring. Sodium carbonate solution (Sigma-Aldrich) as the precipitation agent was added into the mixed Ce^{3+}/Sm^{3+} solution in an appropriate molar ratio, *i.e.* $Ce^{3+}/Sm^{3+} : CO_3^- = 1 : 1.5$, to form a white co-precipitate with the final pH value of the solution being 10–12. The obtained white precipitate was rinsed several times with deionized water, and then washed thoroughly using ethanol followed by drying in an oven at 100 °C overnight and finally ground into powder before sintering at 700 °C for 2 hours.

$LiNO_3$ and $Zn(NO_3)_2 \cdot 6H_2O$ (Sigma-Aldrich) were dissolved in de-ionized water as a 0.5 M solution in various molar ratios. Various amounts of SDC to nominated Li_xZnO powder in a molar ratio of 1∼4 : 1 were added into the Li–Zn sol–gel solution which was stirred and heated at 80 °C on a hot plate to produce the gel mixture. The resultant mixture was stored in an oven at a temperature of 120 °C overnight to form a dried puff gel. Then the above dried gel was calcined at 700 °C for 2 h, resulting in SDC–LiZnO based oxide composite materials.

The solid-state reaction method was adopted to prepare the LiNiCuZn-metal oxide electrodes for fuel cell measurements. A typical composition of Li : Ni : Cu : Zn = 0.15 : 0.2 : 0.25 : 0.4 in terms of the molar ratio was used for the chemicals Li_2CO_3, $NiCO_3 \cdot 3Ni(OH)_2 \cdot 4H_2O$, $Cu_2(OH)_2CO_3$, and $Zn(NO_3)_2 \cdot 6H_2O$ (all chemicals from Sigma-Aldrich). These chemicals were mixed, ground thoroughly, and sintered at 800 °C for 2 h to obtain the electrode materials.

The crystalline phase structure was analyzed using a D/Max-3A Rigaku X-ray diffractometer (XRD) with Co K_α radiation, 35 kV voltage, and 30 mA current. Microstructural characterization of the as prepared samples was performed using a high resolution Philips XL-30 scanning electron microscope (SEM). AC electrochemical impedance spectroscopy (EIS) measurements were performed using a VERASTA 4 (Princeton Applied Research, USA) analyzer under an open circuit voltage from 0.01 Hz to 1 MHz with an amplitude of 10 mV at various temperatures. The curve fitting was made using the ZsimpWin software (Princeton Applied Research, USA).

The fuel cells (FCs) were constructed by a dry-pressing procedure using the as-prepared SDC–Li_xZnO powders as the electrolytes. The fuel cell was constructed in a symmetrical configuration, *i.e.* the same anode and cathode materials, which were prepared respectively by mixing the SDC–Li_xZnO electrolyte and the LiNiCuZn-oxide electrode in a volume ratio of 1 : 1. The FCs were fabricated with 13 mm diameter and 0.7 cm^2 active area. These FCs had a thickness of around 1.0 mm, consisting of an approximately 0.4 mm thick electrolyte layer and 0.6 mm thick electrodes, the anode and cathode being 0.3 mm thick each. Finally, both anode and cathode surfaces were painted with silver paste as the current gets collected for FC measurements. A computerized instrument was used to implement the measurements, data collections and result handling processes. By collecting data of the FC voltage and current under each resistance load, *I* (current)–*V* (voltage) or *I*–*P* (power) curves are plotted.

Results and discussion

XRD analysis was carried out for the composite system between SDC and Li_2O–ZnO in various compositions, denoted as SDC–Li_xZnO. A typical result of SDC–$Li_{0.15}ZnO$ is presented in Fig. 1. At a low Li content, *e.g.* less than 15 mol% ($Li_{0.15}ZnO$), only two phases, the crystallized ZnO (JCPDS no. 70-2551) and doped ceria (JCPDS no. 34-0394), can be detected, while traces of Li_2CO_3 are observed in the high Li content samples, such as SDC–$Li_{0.5}ZnO$,[32] because of the limited solubility of Li in ZnO (around 15 mol%). The cubic SDC has a lattice constant of 5.434 Å, slightly larger than the lattice constant of pure CeO_2 (5.411 Å). In addition, a shift of diffraction peaks to higher angles is observed for all ZnO diffraction signals, which can be

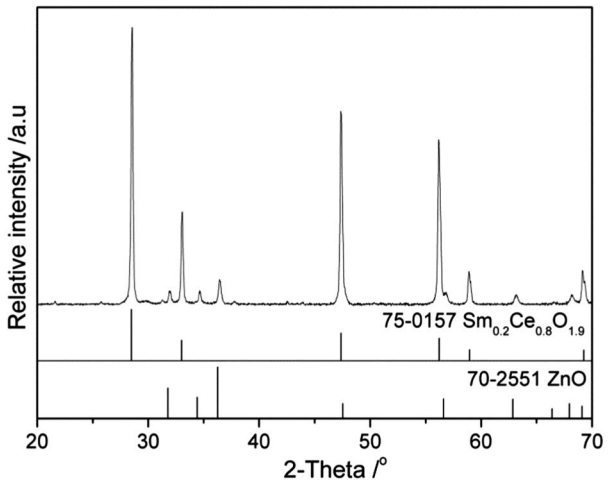

Fig. 1 XRD patterns of SDC–$Li_{0.15}ZnO$. The standard XRD patterns of ZnO and SDC are given for identification. The readers are directed to ref. 32 for the XRD pattern of SDC–$Li_{0.5}ZnO$.

attributed to the presence of the Li dopant on the Zn^{2+} site, leading to the lattice shrinkage of ZnO. The calculated crystal size of doped ceria is 44 nm according to Scherrer's formula.

In a previous study, a clear core–shell structure of SDC coated by Li-doped ZnO has been observed by high-resolution TEM characterization;[32] in the present study such a morphology is observed again in the SEM image, as shown in Fig. 2. The white SDC nanoparticles with a core diameter of less than 100 nm are clearly surrounded by a grey shell of Li_xZnO. The shell is about 15–20 nm in thickness, and uniformly covered on SDC to from a nanocomposite particle size of around 100–120 nm, similar to the SDC–Li_xZnO and SDC–Na_2CO_3 composite electrolytes reported previously.[20,32]

Electrochemical impedance spectroscopy (EIS) was used to determine the electrical conductivity of SDC–(Li_xZnO) composites in air with various Li_2O doped ZnO contents, in order to optimize the composition of the nanocomposites. Fig. 3 shows Arrhenius plots of the Li_xZnO–SDC nanocomposites. The conductivities increase with the increase of the LiZnO content in the composites. In particular, conductivities of samples with LiZnO oxide content less than 25 mol% linearly increase with the decrease of the reciprocal of the absolute temperature. Noticeably, a rapid enhancement of the conductivity takes place between the molar ratios of 1 : 3 and 1 : 2. In addition, a superionic conduction occurs for the SDC–$Li_{0.4}ZnO$ oxide between 300 and 350 °C and SDC–$Li_{0.5}ZnO$ below 300 °C. When the molar ratio of SDC to LiZnO is fixed (1 : 1), the change in the content of Li in LiZnO also leads to different conductivity behaviours as shown in Fig. 3b. The sample with a molar ratio of 1 : 1 between Li and ZnO shows the maximum conductivity in the whole testing temperature range, indicating that the optimized composition of Li_xZnO is 50 mol% each of the dopant and composite in this system. The corresponding activation energies of different samples decrease with the increase of the LiZnO and lithium element content. An incredibly low activation energy of 0.246 eV has been achieved for the SDC–$Li_{0.5}ZnO$ sample, while it is around 1.0 eV for bulk ceria and 0.7 eV for nanoscale samples.[34]

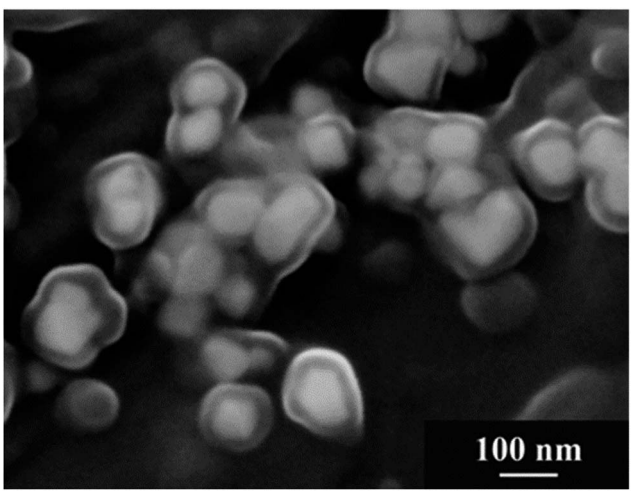

Fig. 2 HR-SEM image of typical core–shel SDC–Li_xZnO.

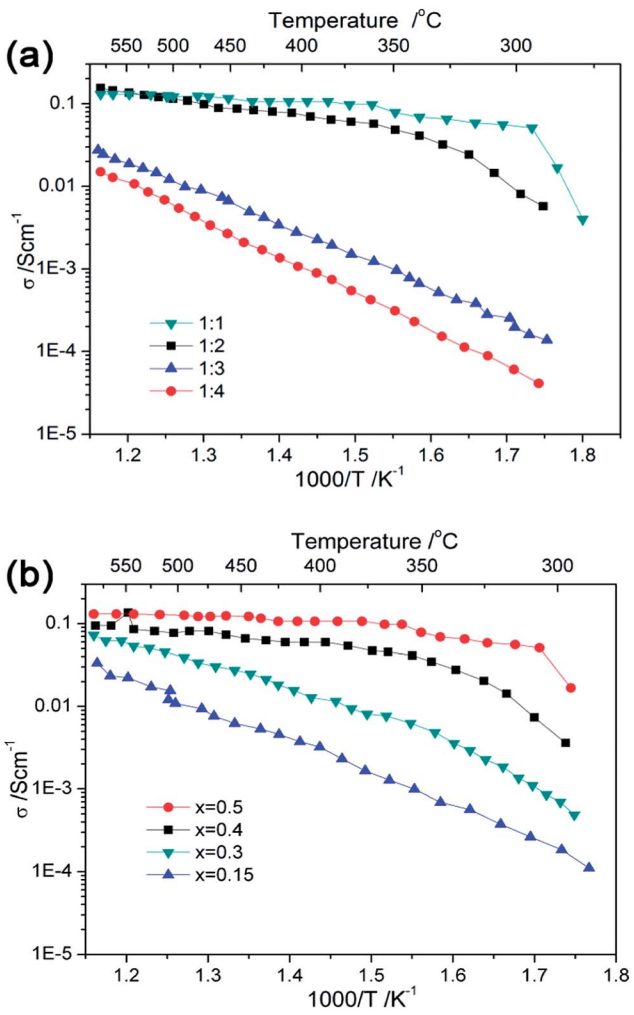

Fig. 3 Arrhenius plots of nanocomposites (a) with different $Li_{0.5}ZnO$ to SDC molar ratios and (b) with various Li contents in Li_xZnO.

To further verify the effective conductivity value measured by EIS, a comparison was carried out between alternating current (AC) EIS conductivities and DC conductivities by fuel cell measurements, as shown in Fig. 4. It is seen that both data are very close above 400 °C. As a matter of fact, the EIS measures mainly intrinsic ions, *e.g.* O^{2-}, which contribute to the conductivity while in DC fuel cell measurements, both intrinsic and extrinsic ions, *e.g.* O^{2-} and H^+, as the source ions make contributions to the conductivity.[23] The slightly higher conductivity data shown in AC conductivity are also ascribed to a possible Li^+ contribution. In other words, it is a common feature that both the intrinsic and the extrinsic ions which depend on the sample *in situ* environments or applied atmospheres contribute to the material conductivity. Thus both AC and DC measurements and comparison of composite material system are necessary. It should also be noticed from Fig. 4 that, below 400 °C, there is a greater difference between the AC and DC results. It may be due to the low catalytic function and increased activation polarization of the electrodes that cause more losses in the DC fuel cell measurements.

Defects theory: intrinsic and extrinsic ions

It can be seen from Fig. 3 and 4 that the best composition of SDC–$Li_{0.5}ZnO$ shows a conductivity value higher than 0.1 S cm^{-2} above 300 °C. The conduction behaviours of this composite may be understood by the defect chemistry theory and the intrinsic and extrinsic ion properties. In ceria, oxygen vacancies ($V_O^{\cdot\cdot}$) can be introduced by doping with oxides of dopants with a lower valence cation, such as Sm^{3+} in this case:

$$Sm_2O_3 \rightarrow 2Sm'_{Ce} + V_O^{\cdot\cdot} + 3O_O^{\times} \quad (1)$$

in which $O_O^{\times}$ is the lattice oxygen, and Sm'_{Ce} indicates that Ce^{4+} is replaced by Sm^{3+}. The O^{2-} (equal to the oxygen vacancy) conductivity has an intrinsic nature which is fixed when the material is prepared with a fixed doping level, 20 mol% Sm in this case.

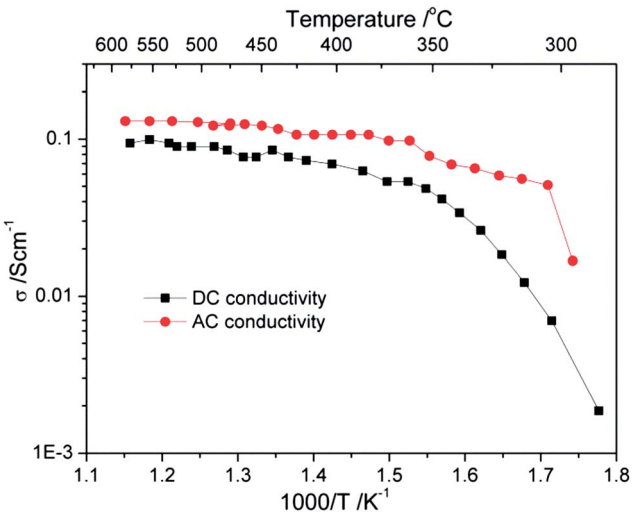

Fig. 4 Comparison of the DC and AC conductivities of SDC–$Li_{0.5}ZnO$ at different temperatures.

In Li_xZnO, the defects depend on Li composition at the doping or mixing level. ZnO structure has complex thermally intrinsic defects, either in the vacancies for both zinc and oxygen, which gives rise to respectively the n and p properties, or Zn and O can also be interstitials, in which case, opposite electrical properties will occur.[35]

For low Li doping levels, normally less than 15 mol% of Li is doped into the ZnO structure, the Li^+ ion doping can result in p-type conductivity and the acceptor defect or $Li_{Zn}^{\times}$ as given below:

$$Li_{Zn}^{\times} \rightarrow Li'_{Zn} + h^{\cdot} \quad (2)$$

The above process will result in p-type conductivity and also a significant lowering of the Fermi level compared to the undoped one.[35] It is well recognized that both the intrinsic and the extrinsic ions play an important role in the material properties in two-phase or multi-phase composite electrolytes, especially in the ceria-based composite materials in fuel cell conditions, where O^{2-} and H^+ ions are commonly present. The intrinsic ion transport is determined by defects formed by doping within a crystal structure, which can even alter the surface/boundary properties in the composite due to surface modifications.

It is very common that the composite electrolytes show *in situ* electrical properties, typically under various gas atmospheres, *e.g.* under air and fuel cell conditions. The former is usually an intrinsic charge carrier and the latter introduces the extrinsic one. The extrinsic ions and the corresponding electrical properties are determined by various parameters, such as the composition, interface area, particle size, morphology and surface properties, having a non-structural nature, *etc.* For example, an extrinsic proton and an additional oxygen vacancy can be produced from an FC anode (H_2) reducing environment; it may be described as

$$2Ce_{Ce}^{\times} + O_O^{\times} \leftrightarrow 2Ce'_{Ce} + V_O^{\cdot\cdot} + 0.5O_2(gas) \quad (3)$$

The oxygen release process can be explained by the redox reaction. The oxygen vacancy and lattice oxygen can further react with water based on the acid–base reaction as mentioned below:

$$(H_2O)_{gas} + V_O^{\cdot\cdot} + O_O^{\times} \leftrightarrow 2OH_O^{\cdot} \quad (4)$$

in which $OH_O^{\cdot}$ is the charge carrier for proton conduction. Water may be produced in the case of H_2 reduction, *e.g.* in the FC case:

$$O_O + 2Ce_{Ce}^{\times} + H_2(gas) \leftrightarrow V_O^{\cdot\cdot} + 2Ce'_{Ce} + H_2O(gas) \quad (5)$$

These processes involve the formation of additional oxygen vacancies and protons in the structure under the reducing atmosphere giving rise to the extrinsic nature of the oxygen ion and proton conductivity. It should be noticed that the SDC–Li_xZnO materials have no structural protons. They only become proton conductors in a hydrogen or water vapour atmosphere. Besides, it can be commonly observed that the two-phase interfaces in the composite materials composed of ceria and the

2nd phase possess an interfacial proton or oxygen ion conduction (see the discussion in the next section). In summary, all intrinsic O^{2-} ions from the ceria (SDC) bulk formed by doping and extrinsic protons generated by the reducing atmosphere or an FC environment can make contributions to electrical conductivities, particularly in the FC case.

Interfacial conduction mechanism

The interfacial conduction mechanism is a key subject in understanding the ion transport phenomena in nanocomposite materials. In the recent research trend, the extremely unusual properties exhibited by the nanocomposites across or along the phase boundaries for electrical, photo-sensitive, voltage, illumination applications and so on have been attracting increasing attention and research efforts of scientists.[36–41] These nanoscale grain boundaries or interfaces have great potential for designing and producing next generation, high efficiency and high power density electronic and electrochemical devices. The nanocomposite SDC–Li_xZnO indeed exhibits such potential towards energy conversion: *e.g.* (i) interfacial superionic conduction, *i.e.* great conductivity enhancement due to the alteration of the two-phase interface area by adjusting the two-phase compositions as shown in Fig. 3 and 4, and (ii) redox reactions can take place on surfaces between the Li_xZnO and SDC particles in the interfaces or phase boundaries, refer to Fig. 6 given below.

Dual oxygen ion and proton conduction in the composite electrolytes has been dealt with extensively from fuel cell measurements.[42–44] Based on the experimental results obtained from different groups, we have proposed different models to study this subject. For example, a Coulombic model was suggested to calculate the interfacial conduction activation energy; an ultra-low activation energy of 0.2 eV for oxygen ion transport at interfaces has been observed.[45] Besides, a Swing model was proposed to explain proton conduction in the ceria–carbonate composite electrolyte, considering the superionic phase transition point and corresponding ultra-low activation energy.[43] From both cases, the interfacial conduction is considered as the key point for the improved ionic conductivity. In order to study the interfacial mechanism and to dig out the origin and scientific description from defect chemistry on this topic, particular attention should be paid to ceria in the ceria-based two- or multi-phase nanocomposites. The Ce^{4+} to Ce^{3+} reduction process in the reducing atmosphere of the FC anode should be emphasized. The nano-ceria surface is more active than that in the bulk, thus the Ce^{4+}/Ce^{3+} redox process may be promoted at nano-particle surfaces or interfaces between ceria and Li_xZnO. In addition, the Ce^{4+}/Ce^{3+} transformation energy was observed to be significantly reduced even by small amounts of the dopant;[46] this effect is magnified when the association between Ce^{3+} ions and oxygen vacancies is taken into account. A similar situation arises in the existence of 2nd phase-Li_xZnO. Considering the nature of both nano-ceria and the composite, there is another possibility that hydrogen or proton could co-exist with the surface Ce^{4+}, which reduces to Ce^{3+}, without forming the oxygen vacancy. Thus H^+ could present as interstitial impurities

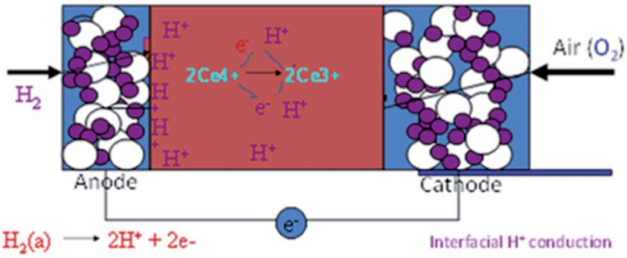

Fig. 5 Scheme of the balance of reduction of Ce^{4+} to Ce^{3+} with H^+ ions without formation of the oxygen vacancy.

to maintain the charge compensation for neutrality. It is very likely that such protons may be formed on the surfaces of the SDC particles[47] and transported at the interface between the SDC and Li_xZnO particles. Fig. 5 presents a scheme of this process for the ceria-based materials in the FC environment: Ce^{4+} is balanced by Ce^{3+} + H^+ equally without forming the conventional oxygen vacancy. The increased proton concentration at the anode side, subsequently on the whole electrolyte layer, may promote the total ionic conduction in the composite electrolyte, which, in fact, has been widely identified as the extrinsic ion transport property in ceria-based composite materials.[23] Moreover, the hydrogen/proton was found to exhibit a very rapid interstitial diffusion rate in ZnO, 8.7×10^{-10} cm^2 V^{-1} s at 300 °C.[48] In the SDC–Li_xZnO case, this interstitial motion may further promote interfacial proton conduction. On the other hand, the interfacial mechanism may be further considered from ion migration activation energies.

The ion transport activation energies of the SDC–Li_xZnO system are calculated and shown in Table 1. It shows a tendency to decrease with increasing Li content, and also the same tendency while increasing the Li_xZnO content up to 50%. This fact may suggest that the interfaces built by introducing the 2nd phase material Li_xZnO in different amounts and the microstructure between the SDC have significant effects on the ionic conduction and migration energy. The core–shell structure seems to be an ideal structure to construct the high ion conduction interfacial channels and at the same time, with the lowest energy needed for ion migration. Co-existence of the Li_xZnO phase alters the SDC surface bonding, defect and interaction situations, and thus also effectively changes the activation energy for oxygen migration which decreases almost monotonically with the Li_xZnO content up to 50 vol%; this indicates facile oxygen diffusion through the bulk or surface

Table 1 Calculated activation energies of composite materials with different $Li_{0.5}ZnO$ and SDC molar ratios, and with different Li contents of SDC–Li_xZnO

Molar ratio	Activation energy/eV	Li content/x	Activation energy/eV
1 : 1	0.246	0.15	0.829
1 : 2	0.456	0.3	0.619
1 : 3	0.822	0.4	0.252
1 : 4	0.938	0.5	0.246

and at the same time creation of an interfacial low energy conducting channel by homogeneous and percolative distributions of the SDC and Li_xZnO, as shown in Fig. 2. In principle, this percolation demands that one of the phases reaches 30 vol%, but it practically depends on the particle size and morphology. Practically synthesized samples could match this percolation in a range of material compositions, *e.g.* in this case, 1 : 1 to 1 : 2. The structural bulk conduction caused by the oxygen ion jump *via* vacancies is the critical cause for the oxygen ion conductivity of ceria single-phase materials. However, the SDC–Li_xZnO composite system is more critically dependent on the interfacial properties formed with various compositions. It may be indicated by the significantly high conductivity observed for the SDC–Li_xZnO composite electrolytes compared to that of each constituent. The superionic transition observed as shown in Fig. 3 is a clear indication that the interface plays a critical role in determining the electrical property of the composite material since each individual phase, *e.g.* the SDC or Li_xZnO, has no phase transition at around 300 °C, besides excellent conductivity, above 0.1 S cm^{-1}, for SDC–Li_xZnO, compared to less than 10^{-4} S cm^{-1} for the SDC and Li_xZnO individual phases. The $0.5Li_2O$–ZnO undergoes a transition at 400 °C, but after that the conductivity rapidly decreases.[49] The SDC–Li_xZnO composite electrolyte showed a superionic conductivity after a transition point at around 300 °C which was maintained at higher temperatures. The oxygen ionic conduction activation energy agrees with the theoretical approach by Zhu *et al.*[45] based on the interfacial conducting mechanisms. Covergence of multiple phases at the nano-level may create great defects (oxygen vacancies/surface oxygen ions), *i.e.* interfaces, thus providing great possibilities for superionic conduction.

The migration of ions in electrolytes is a thermally activated process, where the ionic conductivity (σ) for a solid electrolyte can be described by the Arrhenius equation:

$$\sigma T = \sigma_0 \exp(-E_a/kT) \quad (6)$$

where σ_0 is a pre-exponential factor, E_a the activation energy, k the Boltzmann constant and T is the absolute temperature. The key to designing a superionic conductor is thus to maximize σ_0 and minimize E_a. Besides, the Coulombic model may be used to illustrate the interactions in the interface region, see eqn (7), but the actual interface region is quite complex:

$$E_m = \kappa \frac{1}{4\pi\xi_0\xi} \frac{Qq}{r} \quad (7)$$

where $Q = 2e$ for O^{2-} or $1e$ for O^- and $q = 1e$ for Li^+ or $2e$ for Zn^{2+}, while $\kappa < 1$ because the effective charge between the oxygen ion and the alkaline cation cannot be entirely attributed to the interaction; e is the average dielectric parameter for ceria and carbonate; r is the distance between the M^+ ion of the carbonate and the oxygen ion of ceria.

A Coulombic interaction between the oxygen ion and metal cations is considered and the calculated results are 0.2 eV for O^{2-} and 0.1 eV for H^+ and for the mono-valence metal ions, *e.g.* Li^+; in the case of bivalent cations, such as Zn^{2+}, the activation energies will be double since the formulae in the calculation are proportional to the electrical valence. The SDC–Li_xZnO composite electrolytes show a mono-decreasing dependence of the activation energy by increasing Li molar ratios (Table 1). Since the interfacial migration energy is proportional to the valence of cations and the number of the cations to be interacted with, introduction of a single valence cation, Li^+, thereby directly reducing the cation valance and also the amount of the Zn^{2+} at interfaces, would cause direct reduction of the activation energy. Accompanying this, the superionic conductivity sample SDC–Li_xZnO showed the lowest activation energy, 0.246 eV, which is a typical indication of interface superionic conduction since the structural bulk conduction activation energy is 0.7–1.2 eV, depending on the particle sizes from the nano to the micrometer level.[42]

In the SDC–Li_xZnO system, by increasing the 2nd phase Li_xZnO composition, the system approaches the continuous network for the 2nd phase material, thus causing a steady enhancement of the system conductivity from 20% to 50% continuously. The core–shell structured composite electrolyte showed a maximum conductivity at the intermediate 2nd phase content; a similar situation and composite dependence exist for the SDC–Li_xZnO system, where 50 mol% shows a conductivity above 0.1 S cm^{-1}. At such a composition a continuous network is formed for Li_xZnO, the conductivity reached the maximum and the activation energy dropped to the minimum based on the established interfacial network and interfacial conduction mechanism.

Since the early 90s, ceria has been the best candidate as an alternative for YSZ for reduced temperature SOFCs due to its higher conductivity at lower temperatures. However, ceria behaves as an n-type semiconductor at elevated temperatures and in a reducing atmosphere. This became a big issue in academic R&D during the past several decades, and that is why current industrial applications still use the classical YSZ as the electrolyte.[50,51] The electrons liberated from the reduction reaction are the primary charge carriers as given in the following equation:[52]

$$O_O \leftrightarrow V_O^{\cdot\cdot} + 2e^- + 0.5O_2(g) \quad (8)$$

This should be subtracted from the total conductivity. In the ceria-based composites, introducing the 2nd phase, *e.g.* carbonate, can effectively suppress the electronic conduction by retardation exposure to a reducing gas atmosphere.[16] However, it is an unconvincing explanation, especially when the shell of the composite is a semiconductor, like Li_xZnO. Clearly, a smart and reasonable explanation of the net-electron free phenomenon is of particular interest. It is very essential to understand the exact nature of the underlying processes in these composite systems and to design a scientific approach and methodology based on that to devise and develop new functional materials.

In fact, effort has been devoted to single phase ceria to reduce the electronic conduction at low oxygen partial pressure. One of the unique methods was proposed by Maricle *et al.*[53] in a US patent using a double dopant approach with Pr as the second dopant to trap the electronic charge carriers. Pr possesses good electron trapping capability due to the higher

reduction potential of the Pr^{4+}/Pr^{3+} couple compared with the Ce^{4+}/Ce^{3+} couple. The praseodymium doping lowers the ceria electrolytic domain boundary by two orders of magnitude, to 3.7×10^{-21} atm at 700 °C and results in a decrease of the electronic conductivity by a factor of two under fuel cell conditions.[54] However, this approach is demonstrated to lead to a large increase of the p-type range.[55]

In the present work, we propose an analogous approach to effectively overcome the electronic conductivity of ceria oxide in fuel cell conditions, by introducing a p-conducting 2nd Li_xZnO compound. It should be noted that our approach can not only reduce the electronic conduction but also improve the ionic conductivity. The latter one is of greater significance because it will allow lower temperature operation while it is impossible to reach such a high ionic conductivity value with homogeneous doping to form the solid solution. The electrons can be effectively extracted by hole combinations provided by the p-conducting 2nd phase through an internal or interfacial redox process between the two phase particles, *i.e.* one particle releases an electron, *e.g.* from ceria, and another particle can combine with the electron, *e.g.* p-type Li_xZnO as the 2nd phase. By carefully adjusting the composition, this process could result in the zero net flow of electrons, the so-called net-electron free mechanism. Fig. 6 schematically illustrates such a mechanism and process. This is a unique methodology developed through the NANOCOFC approach. More recent developments based on this interfacial/particle redox and NANOCOFC approaches, new functional ion–semiconductor nanocomposites, have resulted in a new breakthrough technology: the electrolyte-free fuel cell as a research highlight.[30,56–58] We may note that SDC–Li_xZnO reported here or more generally, the ceria–metal oxide composites are a new functional ion–semiconductor system that deserves more future R&D efforts. The methodology described here is unique and has indeed an inherent advantage for the ceria–metal oxide composite electrolytes over the ceria–salt or other all-oxide composites, like SDC–BCY systems.[31]

Fuel cell performances are further demonstrated to show the distinct advantages of such a novel functional material system.

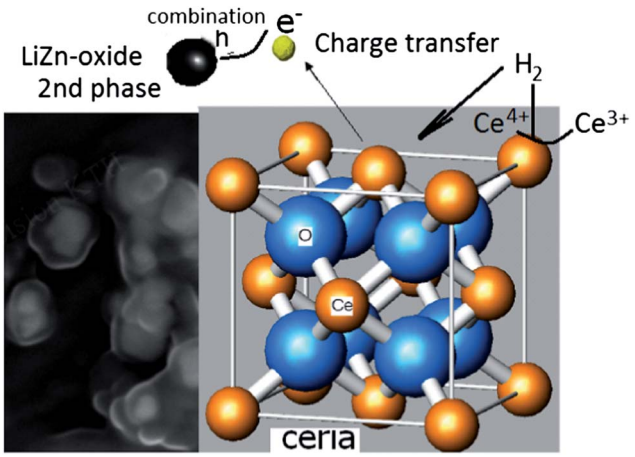

Fig. 6 A schematic illustration of the design mechanism of the composite electrolyte material by the utilization of p-type Li doped ZnO and n-type reduced ceria.

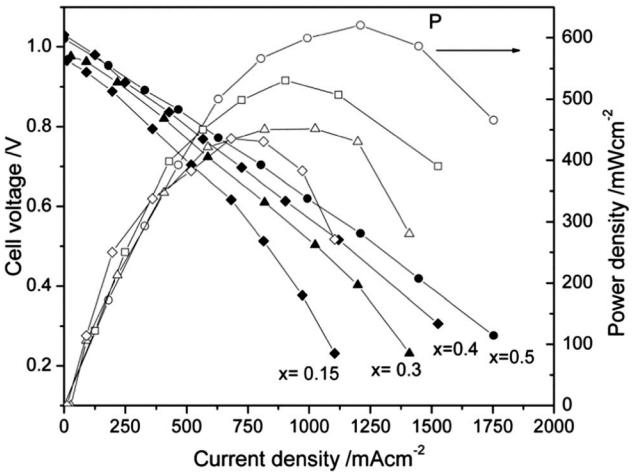

Fig. 7 Electrochemical performance of SOFCs with SDC–Li_xZnO based composite electrolytes at 550 °C.

The *I–V* and *I–P* characteristics measured for various SDC–Li_xZnO electrolytes are shown in Fig. 7. It can be noticed that the power density increases with the increase of the Li content. The maximum power density of 630 mW cm^{-2} has been achieved at 550 °C for the sample SDC–$Li_{0.5}ZnO$. The ratios of Li to Zn may cause the Li_xZnO single phase or yLi_2O–$Li_{x-2y}ZnO$ two mixed phases to further form the SDC–Li_xZnO composites. In the latter case, more interfaces and surfaces could be created to facilitate the interfacial conduction. In addition, the increased Li content will facilitate the formation of p-type Li_xZnO oxide, which will significantly improve the reduction resistance or extract the produced electron by hole combination, and subsequently improve the FC open circuit voltage, as demonstrated in Fig. 7.

Fig. 8 shows the fuel cell performances for SOFCs with different molar ratios of $Li_{0.5}ZnO$ to SDC, where the sample with a molar ratio of 1 : 1 shows the best performance among all samples. The adjustment or change in the composition between the SDC and Li_xZnO can directly affect the interfaces and

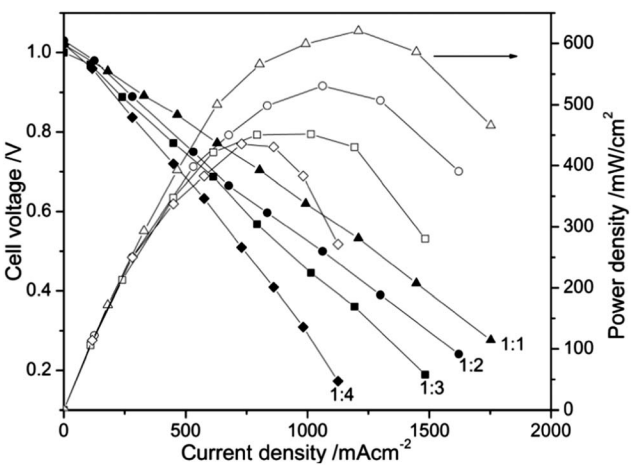

Fig. 8 *I–V* and *I–P* characteristics of the $Li_{0.5}ZnO$–SDC composite electrolyte based SOFCs with different molar ratios of $Li_{0.5}ZnO$ to SDC at 550 °C.

interfacial nature between the constituent phases and subsequently the electrical properties of the composite system. The homogeneous and percolative phase distribution that resulted in large interfaces between Li_xZnO and SDC is likely to play a key role in enhancing the ionic conductivity, up to 0.1 S cm^{-1} around 300 °C, as seen from Fig. 3. The distinguished ionic conductivity will largely reduce the current SOFC operation temperatures.

Fig. 9 illustrates the temperature dependence of electrochemical performances of SOFCs with the SDC–$Li_{0.5}ZnO$ composite electrolyte. The maximum power density is higher than or comparable with that of conventional SOFCs with the ultra-thin and single phase electrolyte at a similar temperature[2,59] Especially, peak performance higher than 400 mW cm^{-2} has been achieved at 480 °C, which is quite promising for practical applications. We should notice that at temperatures below 500 °C, a wide range of cheap metal interconnect and seal materials for stacks exist, which can provide many new viable opportunities for the marketability of LTSOFCs. As a fact, in the current high temperature stack system, these affiliated materials occupy 60% total costs and bring many technical challenges, which are big challenges today being faced by the SOFC community.

The enhanced ionic conductivity of the SDC–LiZnO nanocomposite in this work is ascribed to the interfacial conduction mechanism, which is originated to the interface defects between SDC and LiZnO on the surface of the nanoparticles. There is also another concern, the strained interface, presented in the form of dislocation. In fact, the dislocation, on the other hand, is expected to play an important role in ionic conduction between either two grains (homophase interface) or two different phases (heterophase interface). For example, Huang *et al.*[2] reported the "ion highway project" between highly orientated polycrystalline YSZ and SDC, in an attempt to create dislocations in the crystal structure through which oxygen can move rapidly. In our case, due to the low temperature heat-treatment, the interfacial mechanism has another type of defect, which more probably makes use of planar defects – the surface or grain boundary of nanoparticles in the composite, forming a space charge region that facilitates ionic conduction.[17,60] Compared to structural bulk materials, the unique properties of nanostructured materials are originally from the large amount of planar defects associated with the surface area. In our composite electrolyte, such planar defects on the surface of nanoparticles are utilized as an ionic highway, which is named as the interfacial conduction mechanism. Thus the line defect, *e.g.* dislocation, may play a less significant role in determining the properties of the composite electrolyte.

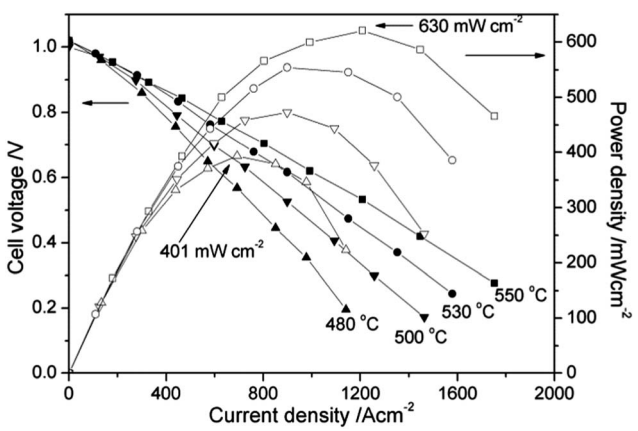

Fig. 9 Temperature dependence of fuel cell performances of the electrolyte material with the best composition SDC–$Li_{0.5}ZnO$.

Conclusions

We have carried out detailed studies on the SDC–Li_xZnO based all-oxide composites as a new functional ion-semiconducting electrolyte for low temperature SOFCs (300–600 °C). The SDC–Li_xZnO composites form homogeneous three dimensional contacts in nano-scale and core–shell structures. The defect studies reveal intrinsic and extrinsic ions and conductivities, especially O^{2-} and H^+ in the fuel cell environment. The ion transport activation energies depended upon the Li : Zn ratio and the SDC : Li_xZnO molar ratios indicate an interfacial conduction mechanism. The nature of the interfacial mechanism, especially for the extrinsic nature of proton conduction, has been emphasized. Based on the interfacial mechanism and the materials of two-phase architecture, we have introduced a 2nd phase with p-type conductivity to combine the electrons released from the ceria in the reducing atmosphere to realize the internal or interfacial redox process on nanoparticles to guarantee that no net electrons flow in the SDC–Li_xZnO composite electrolytes. It thus provides the solution for the technical challenge involving ceria which has remained unsolved even with scientists' extensive R&D efforts over the past several decades. These functional composite materials and methodology development have introduced a new science and technology platform to realize the production of advanced SOFCs that operate in the temperature range of 300–600 °C. Future work will focus on experiments on the conductive behaviours under different oxygen partial pressures and find the possible contribution of the enhanced ionic conductivity from the strained interface (dislocation) by computerized simulation.

Acknowledgements

The Natural Science Foundation of China (NSFC, Grant nos 51072049, 51372075 and 51311130312), the Chinese Scholarship Council (no. 2010625060), the Hubei provincial 100-talent distinguished professor program, the Swedish Research Council (VR, Contract no. 621-2011-4983), the Swedish Agency for Innovation Systems (VINNOVA, Contract no. P36545-1), and the EC FP7 TriSOFC project (Contract no. 303454) are highly appreciated for the financial support.

Notes and references

1 E. Wachsman and K. Lee, *Science*, 2011, **334**, 935.
2 H. Huang, M. Nakamura, P. Su, R. Fasching, Y. Saito and F. B. Prinz, *J. Electrochem. Soc.*, 2007, **154**, B20.

3 P. C. Su, C. C. Chao, J. H. Shim, R. Fasching and F. B. Prinz, *Nano Lett.*, 2008, **8**, 2289.
4 C. Ding and T. Hashida, *Energy Environ. Sci.*, 2010, **3**, 1729.
5 Z. P. Shao and S. M. Haile, *Nature*, 2004, **431**, 170.
6 Y. H. Huang, R. I. Dass, Z. L. Xing and J. B. Goodenough, *Science*, 2006, **312**, 254.
7 L. Yang, S. Z. Wang, K. Blinn, M. F. Liu, Z. Liu, Z. Cheng and M. L. Liu, *Science*, 2009, **326**, 126.
8 M. E. Lynch, L. Yang, W. Qin, J. J. Choi, M. Liu and K. Blinn, *Energy Environ. Sci.*, 2011, **4**, 2249.
9 T. Suzuki, Z. Hasan, Y. Funahashi, T. Yamaguchi, Y. Fujishiro and M. Awano, *Science*, 2009, **325**, 852.
10 M. Liu, M. E. Lynch, K. Blinn, F. M. Alamgir and Y. Choi, *Mater. Today*, 2011, **14**, 534.
11 T. Ishihara, H. Matsuda and Y. Takita, *J. Am. Chem. Soc.*, 1994, **116**, 3801.
12 P. Lacorre, F. Goutenoire, O. Bohnke, R. Retoux and Y. Lallgant, *Nature*, 2000, **404**, 856.
13 H. Inaba and H. Tagawa, *Solid State Ionics*, 1996, **83**, 1.
14 B. C. H. Steele, *Solid State Ionics*, 2000, **129**, 95.
15 S. Wang, T. Kobayashi, M. Dokiya and T. Hashimoto, *J. Electrochem. Soc.*, 2000, **147**, 3606.
16 B. Zhu, *J. Power Sources*, 2003, **114**, 1.
17 B. Zhu, *Int. J. Energy Res.*, 2009, **33**, 1126.
18 B. Zhu, X. Yang, J. Xu, Z. Zhu, S. Ji, M. Sun and J. Sun, *J. Power Sources*, 2003, **118**, 47.
19 J. Huang, Z. Mao, Z. Liu and C. Wang, *Electrochem. Commun.*, 2007, **9**, 2601.
20 X. Wang, Y. Ma, R. Raza, M. Muhammed and B. Zhu, *Electrochem. Commun.*, 2008, **10**, 1617.
21 L. Fan, B. Zhu, M. Chen, C. Wang, R. Raza, H. Qin, *et al.*, *J. Power Sources*, 2012, **203**, 65.
22 C. Xia, Y. Li, Y. Tian, Q. Liu, Z. Wang, L. Jia, Y. Zhao and Y. Li, *J. Power Sources*, 2010, **195**, 3149.
23 A. S. V. Ferreira, C. M. C. Soares, F. M. H. L. R. Figueiredo and F. M. B. Marques, *Int. J. Hydrogen Energy*, 2011, **36**, 3704.
24 X. Li, G. Xiao and K. Huang, *J. Electrochem. Soc.*, 2011, **158**, B225.
25 M. Benamira, A. Ringuedé, V. Albin, R. N. Vannier, L. Hildebrandt, C. Lagergren and M. Cassir, *J. Power Sources*, 2011, **196**, 5546.
26 T. Ristoiu, T. Petrisor Jr, M. Gabor, S. Rada, F. Popa, L. Ciontea and T. Petrisor, *J. Alloys Compd.*, 2012, **532**, 109.
27 L. Fan, C. Wang, M. Chen and B. Zhu, *J. Power Sources*, 2013, **234**, 154.
28 S. Yin, Z. Ye, C. Li, X. Chen and Y. Zeng, *Mater. Lett.*, 2013, **92**, 78.
29 Q. Liu and B. Zhu, *Appl. Phys. Lett.*, 2010, **97**, 183115.
30 B. Zhu, L. Fan and P. Lund, *Appl. Energy*, 2013, **106**, 163.
31 B. Zhu, X. Liu and T. Schober, *Electrochem. Commun.*, 2004, **6**, 378.
32 J. Wu, B. Zhu, Y. Mi, S.-J. Shih, J. Wei and Y. Huang, *J. Power Sources*, 2012, **201**, 164.
33 R. Raza, G. Abbas, X. Wang, Y. Ma and B. Zhu, *Solid State Ionics*, 2011, **188**, 58.
34 M. G. Bellino, D. G. Lamas and N. E. Walsöe de Reca, *Adv. Funct. Mater.*, 2006, **16**, 107.
35 J. G. Lu, Y. Z. Zhang, Z. Z. Ye, Y. J. Zeng, H. P. He, L. P. Zhu, J. Y. Huang, L. Wang, J. Yuan, B. H. Zhao and X. H. Li, *Appl. Phys. Lett.*, 2006, **89**, 112113.
36 J. Seidel, L. W. Martin, Q. He, Q. Zhan, Y. H. Chu, A. Rother, M. E. Hawkridge, P. Maksymovych, P. Yu, M. Gajek, N. Balke, S. V. Kalinin, S. Gemming, F. Wang, G. Catalan, J. F. Scott, N. A. Spaldin, J. Orenstein and R. Ramesh, *Nat. Mater.*, 2009, **8**, 229.
37 S. Y. Yang, J. Seidel, S. J. Byrnes, P. Shafer, C. H. Yang, M. D. Rossell, P. Yu, Y. H. Chu, J. F. Scott, J. W. Ager, L. W. Martin and R. Ramesh, *Nat. Nanotechnol.*, 2010, **5**, 143.
38 O. Diéguez and J. Íñiguez, *Phys. Rev. Lett.*, 2011, **107**, 057601.
39 A. R. Damodaran, C.-W. Liang, Q. He, C.-Y. Peng, L. Chang, Y.-H. Chu and L. W. Martin, *Adv. Mater.*, 2011, **23**, 3170.
40 N. Sata, K. Eberman, K. Eberl and J. Maier, *Nature*, 2000, **408**, 946.
41 J. Maier, *Nat. Mater.*, 2005, **4**, 805.
42 L. Fan, G. Zhang, M. Chen, C. Wang, J. Di and B. Zhu, *Int. J. Electrochem. Sci.*, 2012, **7**, 8420.
43 X. Wang, Y. Ma, S. Li, A.-H. Kashyout, B. Zhu and M. Muhammed, *J. Power Sources*, 2011, **196**, 2754.
44 Y. Zhao, C. Xia, Z. Xu and Y. Li, *Int. J. Hydrogen Energy*, 2012, **37**, 11378.
45 B. Zhu, S. Li and B. E. Mellander, *Electrochem. Commun.*, 2008, **10**, 302.
46 M. G. Bellino, D. G. Lamas and N. E. Walsoe de Reca, *J. Mater. Chem.*, 2008, **18**, 4537.
47 H. Yokokawa, T. Horita, N. Sakai, K. Yamaji, M. E. Brito, Y. P. Xiong and H. Kishimoto, *Solid State Ionics*, 2004, **174**, 205.
48 K. Ip, M. E. Overberg, Y. W. Heo, D. P. Norton, S. J. Pearton, C. E. Stutz, S. O. Kucheyev, C. Jagadish, J. S. Williams, B. Luo, F. Ren, D. C. Look and J. M. Zavada, *Solid-State Electron.*, 2003, **47**, 2255.
49 K. Tsukamoto, C. Yamagishi, K. Koumoto and H. Yanagida, *J. Mater. Sci.*, 1984, **19**, 2493.
50 R. Steinberger-Wilckens, *ECS Trans.*, 2011, **35**, 19.
51 L. Blum, L. G. J. de Haart, J. Malzbender, N. H. Menzler, J. Remmel and R. Steinberger-Wilckens, *J. Power Sources*, 2013, **241**, 477.
52 H. L. Tuller and A. S. Nowick, *J. Phys. Chem. Solids*, 1977, **38**, 859.
53 D. L. Maricle, T. E. Swarr and H. L. Tuller, *US Pat.* 5,001,021, 1991.
54 D. L. Maricle, T. E. Swarr and S. Karavolis, *Solid State Ionics*, 1992, **52**, 173.
55 S. Lübke and H. D. Wiemhöfer, *Solid State Ionics*, 1999, **117**, 229.
56 B. Zhu, R. Raza, G. Abbas and M. Singh, *Adv. Funct. Mater.*, 2011, **21**, 2465.
57 B. Zhu, R. Raza, H. Qin, Q. Liu and L. Fan, *Energy Environ. Sci.*, 2011, **4**, 2986.
58 B. Zhu, R. Raza, H. Qin and L. Fan, *J. Power Sources*, 2011, **196**, 6362.
59 K. Kerman, B. Lai and S. Ramanathan, *Adv. Energy Mater.*, 2012, **2**, 656.
60 E. Fabbri, D. Pergolesi and E. Traversa, *Sci. Technol. Adv. Mater.*, 2010, **11**, 054503.